

Modeling of the Hysteretic $I-V$ Characteristics of TiO_2 -Based Resistive Switches Using the Generalized Diode Equation

Juli Blasco, Nestor Ghenzi, Jordi Suñé, *Fellow, IEEE*, Pablo Levy, and Enrique Miranda, *Senior Member, IEEE*

Abstract—An equivalent circuit representation for the conduction characteristics of TiO_2 -based resistive switches based on the generalized diode equation is reported. The proposed model consists of two antiparallel diodes with series and parallel resistances representing the filamentary current pathway spanning the oxide layer and the possible parasitic conduction effects. The model accounts for the pulse-induced hysteretic behavior exhibited by the $I-V$ characteristic after electroforming. Three different approaches, each one of them with increased complexity, are assessed: 1) constant; 2) nanowire-like; and 3) sigmoidal diode amplitude. In all cases, the logarithmic conductance of the diodes is modeled using a logistic-type threshold function.

Index Terms—Resistive switching, MIM, TiO_2 .

I. INTRODUCTION

DESPITE the major technological advances achieved in the last years in the fabrication of metal-insulator-metal (MIM) information storage cells for nonvolatile memory devices [1], a simple and flexible analytic model able to represent the wide variety of quasi-static current-voltage ($I-V$) characteristics exhibited by resistive switching (RS) devices is still lacking. On the other hand, several models have been proposed to account for the switching dynamics using physics-and/or circuit-based approaches [2]–[8]. Physically, the RS effect in MIM devices has been ascribed to the alternate formation (low resistance state, LRS) and dissolution (high resistance state, HRS) of a filamentary current path spanning the oxide film following a redox process [1]. The filament is initiated by the so-called electroforming process, which is statistically consistent with the percolation theory of oxide breakdown [9]. Interestingly, no clear dependence of both LRS and HRS on the dielectric thickness has been found yet, which is an indication that the current is presumably driven by the narrowest section of the filament regardless of its specific location (bulk or interface). This limitation for the electron

Manuscript received December 6, 2013; accepted December 27, 2013. Date of publication February 3, 2014; date of current version February 20, 2014. This work was supported in part by the Ministry of Science and Innovation under Grant TEC2012-32305 and in part by the DURSI of the Generalitat de Catalunya, Spain, under Grant 2009SGR783. The work of P. Levy was supported in part by the PIP under Grant 20080047 “MeMO,” in part by MeMOSat Project, and in part by CONICET. The review of this letter was arranged by Editor T. Wang.

J. Blasco, J. Suñé, and E. A. Miranda are with the Departament d’Enginyeria Electrònica, Universitat Autònoma de Barcelona, Barcelona 08193, Spain (e-mail: enrique.miranda@uab.cat).

N. Ghenzi and P. Levy are with the Gerencia de Investigación y Aplicaciones, Comisión Nacional de Energía Atómica, Buenos Aires 1872, Argentina.

Color versions of one or more of the figures in this letter are available online at <http://ieeexplore.ieee.org>.

Digital Object Identifier 10.1109/LED.2014.2297992

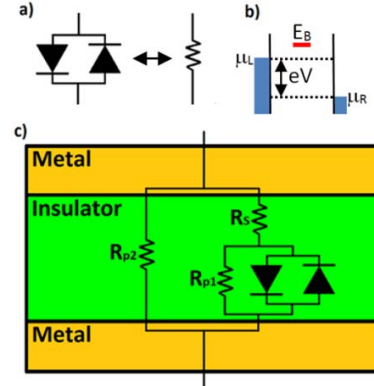


Fig. 1. (a) Szot’s model for the RS mechanism [15]. The two antiparallel diodes and the resistance represent the HRS and LRS states, respectively. (b) Schematic of the potential barrier with height E_B sandwiched between metal electrodes with electrochemical potentials μ_L and μ_R . (c) Equivalent electrical circuit model including series (R_S) and parallel (R_{P1} and R_{P2}) resistances.

flux is often modeled by a material [7], [8], [10]–[12] or virtual [13], [14] potential barrier. In this letter, we modeled the $I-V$ characteristics of TiO_2 -based MIM resistive switches using an extension of Szot’s equivalent electrical circuit for the HRS \leftrightarrow LRS transition [15] [see Fig. 1(a)]. Starting out from the generalized diode equation [16], three different approaches for the hysteretic $I-V$ curves are assessed. The connection with the physics of filamentary conduction is also discussed.

II. EXPERIMENTAL DETAIL

The RS effect in crossbar patterned $\text{Al}(50 \text{ nm})/\text{TiO}_2(50 \text{ nm})/\text{Au}(50 \text{ nm})$ structures was investigated. TiO_2 films were grown by reactive sputtering with a pressure of 20 mTorr and a power of 150 W at room temperature. The bottom (BE) and top (TE) electrodes were deposited by the thermal evaporation method. All the measurements were performed with BE grounded. Three devices with area $100 \mu\text{m}^2$ were electroformed (aprox. -11 V) with current compliances I_{CC} of 50, 100, and $150 \mu\text{A}$. After electroforming the devices exhibited bipolar RS as shown in Fig. 2(a). The RS pulsed $I-V$ characteristics were obtained following a two-step process. First, voltage ramps consisting of pulses (4 ms duration) of increasing/decreasing amplitude with step 25mV, were applied and the current measured. A time interval of 1 s in between pulses was considered in order to minimize the effects of Joule heating of previous pulses [17]. Second, the remnant two terminal resistance was measured in between the pulses by means of a non disturbing constant voltage at 0.1 V. Fig. 2(b) illustrates the resistance hysteresis switching loop for different compliance values.

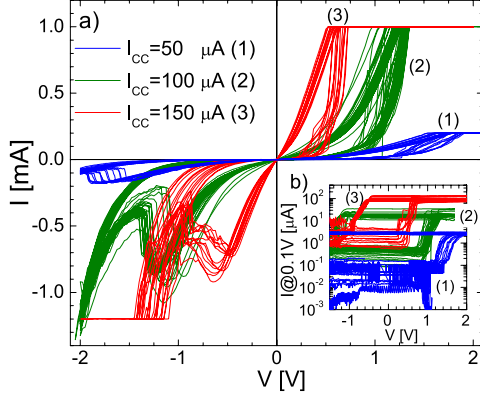


Fig. 2. (a) I - V characteristics measured in Al/TiO₂/Au structures after electroforming with different current compliances I_{CC} . (b) Resistance hysteresis switching loops associated with the curves shown in (a). Current compliances are used to limit the degradation of the device.

III. MODEL DESCRIPTION AND FITTING RESULT

According to quantum theory, the current that flows through a nanojunction characterized by a tunneling barrier or subband structure of height E_B can be approximated by the expression [18]:

$$\begin{aligned} I &= I_{L \rightarrow R} - I_{R \rightarrow L} \\ &\approx A \left\{ \exp[-\gamma(E_B - \mu_L)] - \exp[-\gamma(E_B - \mu_R)] \right\} \quad (1) \end{aligned}$$

where A and γ are constants that depend on the particular features of the barrier shape and injection mechanism considered [19]. μ_L and μ_R are the electrochemical potentials at the left and right reservoirs of the junction, respectively [see Fig. 1(b)]. Under the application of a positive bias $V > 0$, $\mu_L - \mu_R = eV$ so that (1) can be rewritten as:

$$I(V) \approx I_0 [\exp(\beta V) - 1] \quad (2)$$

which is formally equivalent to the ideal diode equation. $I_0 = A \exp(-\beta \Phi)$ is referred to as the diode amplitude, Φ is the barrier height with respect to μ_R , e the electron charge and $\beta \approx d \ln(I)/dV$ the logarithmic conductance of the diode, *i.e.* the slope of the I - V curve in log-linear axes. For $V < 0$ a similar equation, with the appropriate signs, holds. As pointed out in [18], for $\beta \ll 1$, $I(V) \approx A\beta V$, thus the potential barrier is associated with a resistance $(A\beta)^{-1}$. This is consistent with the diode-resistor transition depicted in Fig. 1(a), but at variance with the magnitude of I expected in either case. Notice that for $E_B < \mu_L$, the barrier vanishes for part of the electron injection window which can, in principle, accommodate a linear I - V characteristic with the right magnitude. In this regard, the barrier height modulation is the physical mechanism behind the quantum point-contact (QPC) model for RS devices [13]. In order to extend Szot's approach for RS [15] to other material systems than the one considered here, for the sake of generality, series (R_S) and parallel resistances (R_{P1} , R_{P2}) are included in the circuit model. Physically, R_S may represent a remnant local potential barrier, while R_{P1} and R_{P2} may represent localized and area distributed parallel leakage current pathways, respectively [10], [11].

From (2) and Fig. 1(c), the corresponding equation reads:

$$\begin{aligned} I(V) &= I_0 \{ \exp[\beta(V(1 + R_S G_{P2}) - IR_S)] - 1 \} \\ &\quad - I_0 \{ \exp[-\beta(V(1 + R_S G_{P2}) + IR_S)] - 1 \} \\ &\quad + (V - IR_S) G_{P1} + VG_{P2}(1 + R_S G_{P1}) \quad (3) \end{aligned}$$

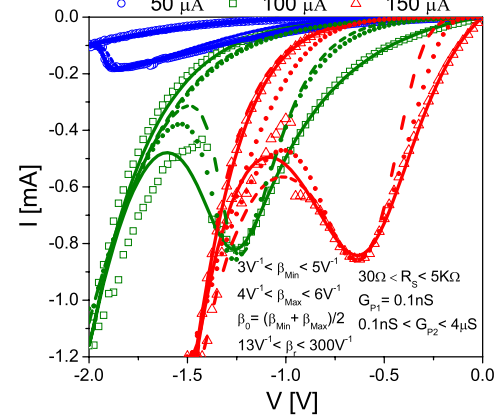


Fig. 3. Experimental I - V (symbols) and model (lines) results in the negative bias region for the three compliances investigated. Dotted, dashed and solid lines correspond to approaches *a*), *b*) and *c*), respectively.

where $G_{P1} = 1/R_{P1}$ and $G_{P2} = 1/R_{P2}$. Assuming that each diode is active at a time, (3) can be solved using the Lambert- W function as [16]:

$$I(V) = \text{sgn}(V) \left\{ (\beta R_S)^{-1} W \left[\beta I_0 R_S \kappa \exp(\beta \kappa(|V| + I_0 R_S)) \right] \right. \\ \left. + \kappa(|V| G_{P1} - I_0) - |V| G_{P2} \right\} \quad (4)$$

where $\kappa = (1+G_{P1}R_S)^{-1}$, sgn is the sign function and $|x|$ is the absolute value of x . In this letter, the logarithmic conductance of the diodes is modeled using the threshold function:

$$\beta(V) = \beta_{Min} + \frac{\beta_{Max} - \beta_{Min}}{1 + \left(\frac{\beta_{Max} - \beta_0}{\beta_0 - \beta_{Min}} \right) \exp[-\beta_r V_\phi]} \quad (5)$$

which provides a continuous transition $\beta_{Min} \leftrightarrow \beta_{Max}$ during the application of the voltage sweep [20]. β_{Min} , β_{Max} , β_r , and $\beta_{Min} < \beta_0 < \beta_{Max}$ are the maximum, minimum, switching rate, and initial value of β , respectively. V_ϕ is the applied voltage with an additional phase shift. This parameter determines the set and reset voltages at which the transition HRS \leftrightarrow LRS takes place. Since $\beta = \beta(V)$, notice that (4) is strictly valid for the steady values $\beta = \beta_{Min}$ and $\beta = \beta_{Max}$. In what follows, three particular approaches for the diode amplitude are assessed.

A. Constant Amplitude (Dotted Line in Fig. 3)

For I_0 constant, (3) can be expressed as:

$$I(V) = 2I_0 \sinh[\beta(V(1 + R_S G_{P2}) - IR_S)] \\ + (V - IR_S) G_{P1} + VG_{P2}(1 + R_S G_{P1}) \quad (6)$$

which corresponds to the models reported in [21] and [22] with $R_S = 0$ and $R_{P1} = R_{P2} = \infty$. Since there is no relationship between I_0 and β , in general, it is hard to capture the behavior of the LRS and HRS I - V curves in the whole bias range. However, this approach is useful for modeling the transition between two nonlinear I - V curves that are not too far apart. As shown in Fig. 3, the deviation from the experimental data can be significant if one attempts to reproduce the negative differential resistance region accurately. The deviations can be compensated in part using the series and shunt resistances.

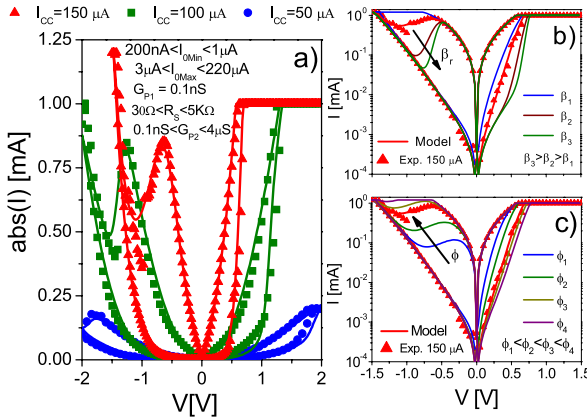


Fig. 4. (a) Experimental and theoretical I - V characteristics calculated using approach (c) for three current compliances. (b) Effect of the transition rate β on the I - V curves. (c) Effect of the phase shift ϕ on the I - V curves.

B. Quantum-Wire Amplitude (Dashed Line in Fig. 3)

Alternatively, (6) can be expressed as:

$$I(V) = 2I_m \frac{\exp(-\beta\Omega)}{\beta} \sinh[\beta(V(1 + R_S G_{P2}) - IR_S)] + (V - IR_S) G_{P1} + VG_{P2}(1 + R_S G_{P1}) \quad (7)$$

so that $I_0 = I_m \exp[-\beta\Omega]/\beta$ in (4). I_m and Ω are fitting constants. (7) closely resembles the expression for the current given by the QPC model in the soft-breakdown mode [20]. Notice also that (7) is similar to (2) and to the gap modulation model of Guan *et al.* [8] except for the factor β in the denominator of I_0 . Moreover, for $\Omega = 0$, the expression for the RS I - V characteristics in solid electrolytes is obtained [23]. Now, β and I_0 are correlated: a lower logarithmic conductance is associated with larger diode amplitude. In the limit $\beta \rightarrow 0$ (LRS), (7) yields a linear I - V independent of β and Ω , key parameters for setting both the HRS current magnitude and its slope. This approach is suitable for modeling the transition between exponential (HRS) and linear (LRS) I - V curves.

C. Sigmoidal Amplitude (Solid Lines in Figs. 3 and 4)

In this case I_0 in (4) is driven by an expression similar to (5) but with parameters I_{0Max} , I_{0Min} , I_{0r} , and $I_{0Min} < I_0 < I_{0Max}$. This is a physically unrestricted approach. Since the number of parameters increases significantly this approach provides the best fitting results in the whole bias range for the three current compliances considered in this letter [see Fig. 4(a)]. As illustrated in Fig. 4(b) and (c), the model nicely fits the I - V characteristics in log-linear axis as well. Notice the effect of β_r and ϕ on the model curves. When I_0 and β are in phase, the model can deal with the switching between two exponential I - V curves. However, if the sigmoidals are in counterphase, the model can represent the switching between an exponential and a linear I - V .

IV. CONCLUSION

An equivalent circuit for the hysteretic I - V characteristics of TiO_2 -based MIM structures after electroforming was presented. The model extends Szot's circuital description for RS, incorporating series and parallel resistances and a threshold function to account for the transition between the high and low resistance states. This basic approach can

be further extended by including memory effects, aging effects, stochasticity, etc., on the model parameters as well as physics-based switching rules for the threshold function.

REFERENCES

- [1] R. Waser, R. Ditmann, G. Staikov, *et al.*, "Redox-based resistive switching memories—Nanoionic mechanisms, prospects, and challenges," *Adv. Mater.*, vol. 21, nos. 25–26, pp. 2632–2663, Jul. 2009.
- [2] D. Jeong, H. Schroeder, and R. Waser, "Mechanism for bipolar switching in a Pt/TiO₂/Pt resistive switching cell," *Phys. Rev. B*, vol. 79, no. 19, pp. 195317-1–195317-10, May 2009.
- [3] B. Gao, J. Kang, Y. Chen, *et al.*, "Oxide-based RRAM: Unified microscopic principle for both unipolar and bipolar switching," in *Proc. IEEE IEDM*, Dec. 2011, pp. 417–420.
- [4] R. Degreave, A. Fantini, S. Clima, *et al.*, "Dynamic 'hour glass' model for SET and RESET in HfO₂ RRAM," in *Proc. Symp. VLSI Technol.*, Jun. 2012, pp. 75–76.
- [5] Z. Bielek, D. Bielek, and V. Biolkova, "SPICE model of memristor with nonlinear dopant drift," *Radioengineering*, vol. 18, no. 2, pp. 210–214, 2009.
- [6] D. Ielmini, "Modeling the universal set/reset characteristics of bipolar RRAM by field- and temperature-driven filament growth," *IEEE Trans. Electron Devices*, vol. 58, no. 12, pp. 4309–4317, Dec. 2011.
- [7] S. Menzel, U. Bottger, and R. Waser, "Simulation of multilevel switching in electrochemical metallization memory cells," *J. Appl. Phys.*, vol. 111, no. 1, pp. 014501-1–014501-5, Jan. 2012.
- [8] X. Guan, S. Yu, and H.-S. P. Wong, "A SPICE compact model of metal oxide resistive switching memory with variations," *IEEE Electron Device Lett.*, vol. 33, no. 10, pp. 1405–1407, Oct. 2012.
- [9] S. Long, C. Cagli, D. Ielmini, *et al.*, "Analysis and modeling of resistive switching statistics," *J. Appl. Phys.*, vol. 111, no. 7, pp. 074508-1–074508-19, Apr. 2012.
- [10] J. Borgetti, D. B. Strukov, M. D. Pickett, *et al.*, "Electrical transport and thermometry of electroformed titanium dioxide memristive switches," *J. Appl. Phys.*, vol. 106, no. 12, pp. 124504-1–124504-5, Dec. 2009.
- [11] W. Yi, F. Perner, M. Qureshi, *et al.*, "Feedback write scheme for memristive switching devices," *Appl. Phys. A*, vol. 102, no. 4, pp. 973–982, Mar. 2011.
- [12] J. Hur, M. Lee, C. Lee, *et al.*, "Modeling for bipolar resistive memory switching in transition-metal oxides," *Phys. Rev. B*, vol. 82, no. 15, pp. 155321-1–155321-5, Oct. 2010.
- [13] E. Miranda, C. Walczyk, C. Wenger, *et al.*, "Model for the resistive switching effect in HfO₂ MIM structures based on the transmission properties of narrow constrictions," *IEEE Electron Device Lett.*, vol. 31, no. 6, pp. 609–611, Jun. 2010.
- [14] V. Zhirnov, R. Meade, R. K. Cavin, *et al.*, "Scaling limits of resistive memories," *Nanotechnology*, vol. 22, no. 25, pp. 254027–254048, Jun. 2011.
- [15] K. Szot, W. Speier, G. Bihlmayer, *et al.*, "Switching the electrical resistance of individual dislocations in single-crystalline SrTiO₃," *Nature Mater.*, vol. 5, pp. 312–320, Mar. 2006.
- [16] A. Ortiz-Conde, F. García-Sánchez, and J. Muci, "Exact analytical solutions of forward non-ideal diode equation with series and shunt parasitic resistances," *Solid-State Electron.*, vol. 44, no. 10, pp. 1861–1864, Jan. 2000.
- [17] N. Ghenzi, M. Sánchez, and P. Levy, "A compact model for binary oxides-based memristive interfaces," *J. Phys. D, Appl. Phys.*, vol. 46, no. 41, pp. 415101-1–415101-3, Oct. 2013.
- [18] D. Segal and A. Nitian, "Heating in current carrying molecular junctions," *J. Chem. Phys.*, vol. 117, pp. 3915–3927, Aug. 2002.
- [19] D. K. Ferry, S. M. Goodnick, and J. Bird, *Transport in Nanostructures*, 2nd ed. Cambridge, U.K.: Cambridge Univ. Press, 2009.
- [20] E. Miranda, D. Jiménez, and J. Suñé, "The quantum point-contact memristor," *IEEE Electron Device Lett.*, vol. 33, no. 10, pp. 1474–1476, Oct. 2012.
- [21] J. Simmons and R. Verderber, "New conduction and reversible memory phenomena in thin insulating films," *Proc. R. Soc. London Ser. A, Math. Phys. Sci.*, vol. 301, no. 1464, pp. 77–102, Oct. 1967.
- [22] C. Rossel, G. I. Meijer, D. Bremaud, *et al.*, "Electrical current distribution across a metal–insulator–metal structure during bistable switching," *J. Appl. Phys.*, vol. 90, no. 6, pp. 2892–2898, Sep. 2001.
- [23] M. Morales-Masis, H.-D. Wiemhofer, and J. M. van Ruitenbeek, "Towards a quantitative description of solid electrolyte conductance switches," *Nanoscale*, vol. 2, no. 10, pp. 2275–2280, Aug. 2010.